Progress In Electromagnetics Research C, Vol. 83, 205–216, 2018

Experimental Investigation of Space and Polarization Characteristics of a Subway-Like Tunnel Channel

Xiaoyu Yin* **and Guoxin Zheng**

Abstract—This article studies the spatial domain and polarization domain characteristics of multipath channels in a subway-like tunnel environment. Experiments were performed by rotating a horn antenna with 30° half power beamwidth (HPBW) in the azimuthal direction for two different transmitter-receiver (Tx-Rx) distances. The time domain measurement is conducted when carrier frequency is set as 1.8 GHz. The cross-polarization discrimination (XPD) is studied, and it is found that the maximum depolarized signals are from sidewalls. The characteristics of power azimuth spectrum (PAS) of co-polarized and cross-polarized signals follow a multi-cluster Gaussian distribution. Ray-tracing method is employed to investigate the wave propagation in the tunnel environment. The results demonstrate that the main multipath components (MPCs) are around the line-of-sight (LOS) direction, and the reflected waves are from the other end of the tunnel (RWET). The correlation coefficient of co-polarized configuration pursues an increasing function with respect to the Tx-Rx distance and a decreasing function with respect to the cross-polarized configuration.

1. INTRODUCTION

Urban rail transit systems are developing rapidly in China. Long Term Evolution for Metro (LTE-M) operating at frequency band of $1,795\,\text{MHz} \sim 1,805\,\text{MHz}$ has been proposed to meet the advanced communication requirement [1]. Multiple-input multiple-output (MIMO) can increase channel capacity without increasing transmit power and frequency resources, and is one of the key technologies for LTE-M. The environment in a tunnel is complicated and requires an accurate investigation of the signal propagation.

Single-input single-output (SISO) channel of underground tunnels has been extensively explored in terms of theory and experiments [2, 3]. Path loss and delay spread are the main focus of the SISO channel. To attain higher data rates and good efficiency, Lienard et al. pioneered a study of MIMO channel in a subway tunnel environment, and they explained the antenna array configuration, tunnel orientation and the antenna spacing effects on the performance of MIMO systems comprehensively [4]. In [5], the consequences of antenna spacing and height on the performance of a MIMO system were considered thoroughly for the tunnel environment. The research in [6] found that the antenna array position and tunnel aspect ratio have a significant influence on the MIMO channel capacity. The impact of antenna polarization on the MIMO system is vital. The influence of polarization diversity on MIMO channel performance was investigated in [7, 8] in subway tunnel environments. The results reveal that for a fixed signal-to-noise ratio (SNR), cross-polarized channel capacity is higher than that of co-polarized channel. For a MIMO channel, spatial domain is as important as polarization domain. Power azimuth spectrum (PAS) is defined as the spatial distribution of azimuth received power. Angular spread (AS) is

Received 6 February 2018, Accepted 9 April 2018, Scheduled 24 April 2018

* Corresponding author: Xiaoyu Yin (ytuyxy@163.com).

The authors are with the Key Laboratory of Specialty Fiber Optics and Optical Access Networks, Joint International Research Laboratory of Specialty Fiber Optics and Advanced Communication, Shanghai Institute for Advanced Communication and Data Science, Shanghai University, China.

the standard deviation of PAS. The relation between the AS and MIMO channel correlation coefficient is studied. Larger AS results in a lower MIMO correlation coefficient. AS was experimentally studied in [9] for a large arched road tunnel in the Massif Central in south-central France. The results in [9] reveal that AS is a decreasing function of transmitter-receiver (Tx-Rx) distance. In [10], based on the waveguide theory, it was shown that the Gaussian distribution fitted well for PAS, and the AS characterization is the same as in [9]. In [11], co-polarized angular characterization was studied in the Nantong tunnel without considering the reflected wave from the other end of the tunnel (RWET), and the results reveal that the greater the Tx-Rx distance is, the lower the AS will be. However, there was a lack of PAS information in [11]. To the best of our knowledge, the angle-of-arrival (AoA) of cross-polarized signals in tunnels are not reported yet. The joint space and polarization diversities have been proposed as an attractive method to boost the MIMO system capacity [12]. In this research, we fill the gap by investigating the joint space and polarization channel characterization. Since the actual subway tunnel operates for a longer time daily, for safety purpose we were not allowed to get in the tunnel easily. We carried out a channel measurement campaign in a subway-like tunnel and give an analysis of the experiment results. The cross-polarization discrimination (XPD), PAS, AS and spatial correlation were investigated in two different Tx-Rx distances for co-polarized and cross-polarized configurations.

The rest of this paper is structured as follows. Section 2 deals with the measurement campaigns conducted in the Nantong tunnel. Data processing and analysis are given in Section 3. Finally, Section 4 draws the conclusion.

2. MEASUREMENTS

2.1. Measurement Setup

The time domain pseudo-noise (PN) correlation method was adopted in the measurements. The measurement setup is shown in Fig. 1. In Keysight E8267D vector signal generator (VSG), a PN sequence with 511 chips was transmitted periodically with a transmission rate of 40.8 Mega chip-per-second (Mcps). The PN sequence was modulated with Binary Phase Shift Keying (BPSK) and up-converted to the carrier frequency of 1.8 GHz. The transmit power was set to 20 dBm. After the wireless signal was received, it was down-converted and digitized with a sampling rate of 81.6 MHz in Rohde & Schwarz (R&S) FSG8 spectrum analyzer (SA). During measurement, the high-stability 10 MHz Rubidium reference clock synchronization signal was transmitted to both the transmitter (Tx) and receiver (Rx).

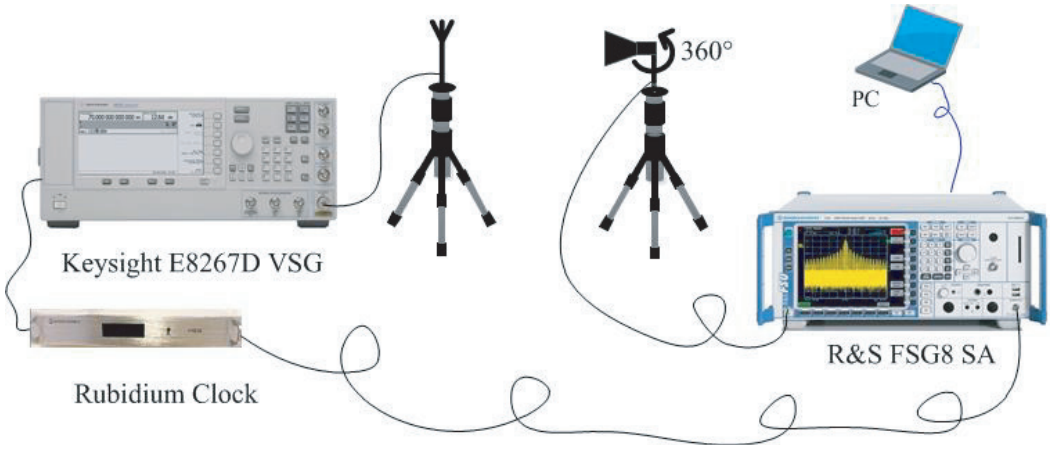

Figure 1. Channel sounding setup.

The Tx antenna is an omnidirectional bi-conical antenna (A-INFOMW SZ-50300/P) with the gain of 0 dBi. The Tx antenna is vertically polarized. The Rx antenna is a dual-polarized open boundary quad-ridged horn antenna (A-INFOMW LB-OSJ-0760-SF) with a gain of 11 dBi. The half-power beamwidth (HPBW) of the Rx antenna at 1.8 GHz is about 30°. The measurement parameters are

Table 1. Channel measurement parameters.

Description	Value
Center frequency	1.8 GHz
Transmitting power	20 dBm
Bandwidth	40.8 MHz
Sample rate	81.6 MHz
Delay resolution	24.5 ns
Maximum delay	12524.5 ns
Sounding signal	PN sequence
PN sequence length	511 chips
Tx antenna	Bi-conical
Rx antenna	Horn
HPBW of Rx antenna	30°
Tx antenna gain	0 dBi
Rx antenna gain	11 dBi
Antenna height	1.6 m

summarized in Table 1. The Rx antenna was rotated from 0° to 360° with an evenly separated azimuth angle of 10°. For each measurement angle, 2000 channel realizations were collected to guarantee the reliability of the measured data. Two types of polarization configurations (VV, VH) for the channel measurements were performed throughout our experiments.

VV (co-polarized configuration): both the Tx and Rx antennas are vertically polarized.

VH (cross-polarized configuration): Tx antenna is vertically polarized, and Rx antenna is horizontally polarized.

2.2. Measurement Environment

The measurements were conducted in a subway-like tunnel in Zhongtian technology Company (ZTT), Nantong, China. The tunnel functions for electromagnetic experiments. The tunnel length is 100 m, in which 50 m is rectangle with the cross-section of 4.4 m×3 m, and the other 50 m is an arch with a radius of 1.95 m. At the other end of the tunnel, there is a metal door with size of $1.76 \times 2.38\,\mathrm{m}^2$. The tunnel wall is made of reinforced concrete material, and nobody was moving throughout the measurements. The tunnel wall materials have the same characteristics as the actual subway tunnels. Fig. 2 shows the

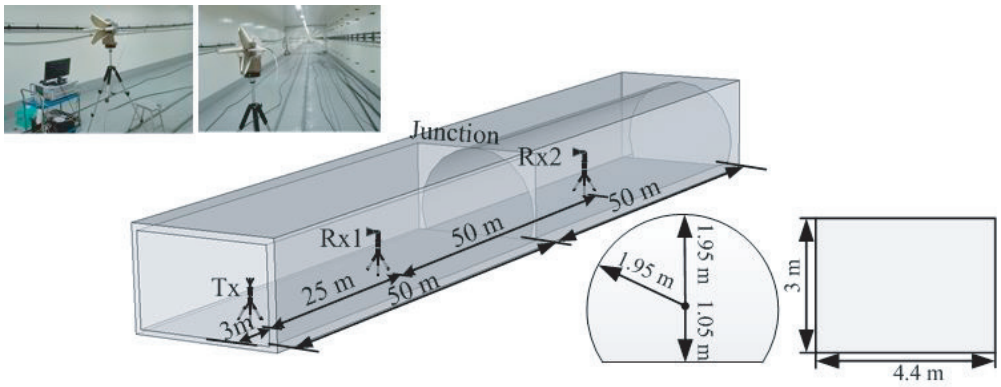

Figure 2. Layout of the measurement scenarios.

layout of the channel measurements in the tunnel. The Tx was fixed at 3 m away from the entrance. The Rx changed its position from Rx1 to Rx2, of which the distance varies from 25 m to 75 m far from the Tx, respectively.

3. RESULTS AND ANALYSIS

The channel impulse response is directly generated by cross-correlating the collected data with the replica of transmitted sequence [13]. To separate the valid multipath components (MPCs) from the background noise, the threshold was calculated based on a 5 dB signal-to-noise (SNR) threshold relative to the mean thermal noise floor of the raw power delay profile [14].

3.1. Characterization of XPD

The XPD is expressed as the ratio of co-polarized received power to the cross-polarized received power [15]

$$\mathbf{XPD}(\phi) = 10 \cdot \log_{10} \left\{ \frac{P_{VV}(\phi)}{P_{HV}(\phi)} \right\} \text{ (dB)} \tag{1}$$

where $P_{ij}(\phi)$ denotes the power of j-to-i polarization with the azimuth AoA of ϕ. Fig. 3 shows the XPDs with the transmitter-receiver (Tx-Rx) distance of 25 m and 75 m, and the shape of the curve appears similar to the capital letter "W". It should be noted that the direction of reference $\phi = 0°$ is defined as the direction of the Rx pointing towards the Tx. The positive azimuth angle represents that the Rx antenna rotates in a clockwise direction, and the negative azimuth angle means a counter-clockwise rotation.

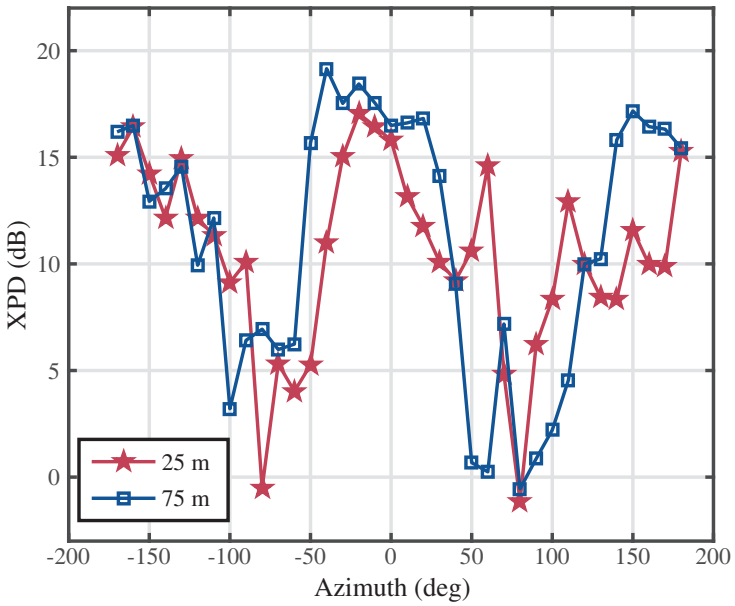

Figure 3. Cross-polarization discrimination.

At 25 m, the maximum depolarization is respectively around $60° < \phi < 100°$ and $-90° < \phi < -50°$. These two MPC clusters cover the signals that are the reflection waves from the sidewalls (RWS), and both are completely depolarized. At 75 m, the maximum depolarization is around $30° < \phi < 130°$ and $-110° < \phi < -50°$. The XPD values are even negative when $\phi = \pm 180°$ at 25 m and $\phi = 80°$ at 75 m, respectively.

Due to reflection from the tunnel wall, the electric field direction of the electromagnetic wave is rotated, and the polarization direction is reversed at the Rx. For RWS, the waves experience multi-reflections and are considered as totally depolarized. However, the RWET is known as the first-order

reflection wave and partially depolarized wave. Therefore, the depolarization of the RWET is trivial compared to RWS. So the curve presented in Fig. 3 is like a "W" shape. For the two scenarios with different Tx-Rx distances, the depolarization almost shows the same varying trend. The only difference is that the maximum depolarized angle range at 75 m is a little larger than that at 25 m. The main reason for this distinction is that the RWS becomes weaker with increasing Tx-Rx distance.

3.2. Power Azimuth Spectrum (PAS)

From the measurement results, the multi-cluster Truncated Gaussian distribution is found to be the best fit for the measured PAS. Using nonlinear least square distribution fitting, the multi-cluster PAS for co-polarized and cross-polarized signals within different Tx-Rx distances can be modeled as:

$$P(\phi) = \sum_{n=1}^{M} \frac{Q_n}{\sqrt{2\pi\sigma_n^2}} e^{\frac{-1}{2\sigma_n^2}(\phi-\phi_n)^2}, \tag{2}$$

for the n-th cluster, $-\Delta\phi_n+\phi_n \leq \phi \leq \Delta\phi_n+\phi_n$, M is the number of clusters, ϕ the azimuth angle, σ_n the azimuth AS of the n-th cluster, and ϕ_n the mean azimuth AoA of the n-th cluster, $Q_n = erf(\Delta\phi_n/\sqrt{2}\sigma)$.

Figures 4–7 show the multi-cluster Gaussian distribution fitted to PAS obtained through the channel measurements in the subway-like tunnel. For co-polarized configurations, two clusters with mean azimuth AoA of 0° and 180° are received at the Rx. The AS for both clusters decreases when the Tx-Rx distance increases. In [10], RWET does not exist. We find that the line-of-sight (LOS) cluster PAS characterization of the co-polarized configuration in the tunnel is the same as the theoretical studied one in [10].

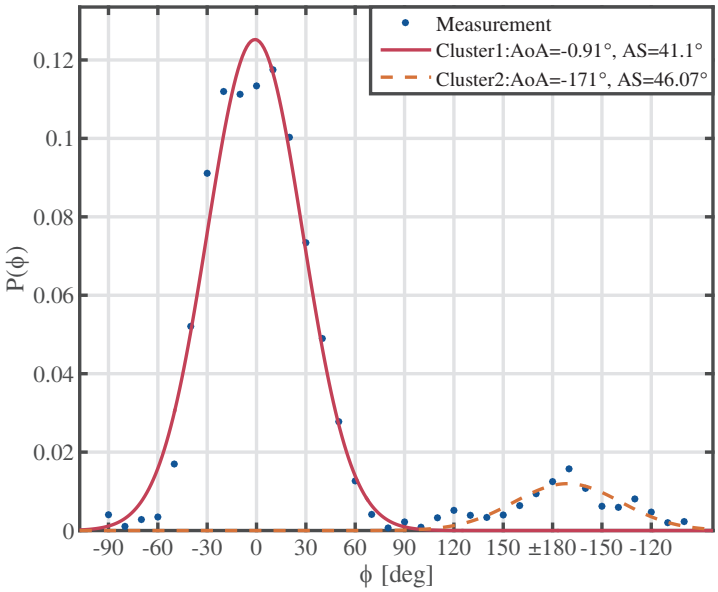

Figure 4. Co-polarized PAS for Tx-Rx distance of 25 m.

For cross-polarized configurations, the number of clusters is greater than the co-polarized configurations due to the reflection property for depolarization. Since there is no LOS propagation, the Rx has a limited dynamic range, and the reflected wave that has lower power can be detected by the Rx. The AS for the cluster of the highest power has larger AS than that of the other clusters (except the RWET cluster).

3.3. Power Angle Profile (PAP)

We used ray-tracing method to investigate the azimuth AoA for the multipath propagation in the tunnel environment. We used the Wireless InSite (WI) software which is for the electromagnetic wave

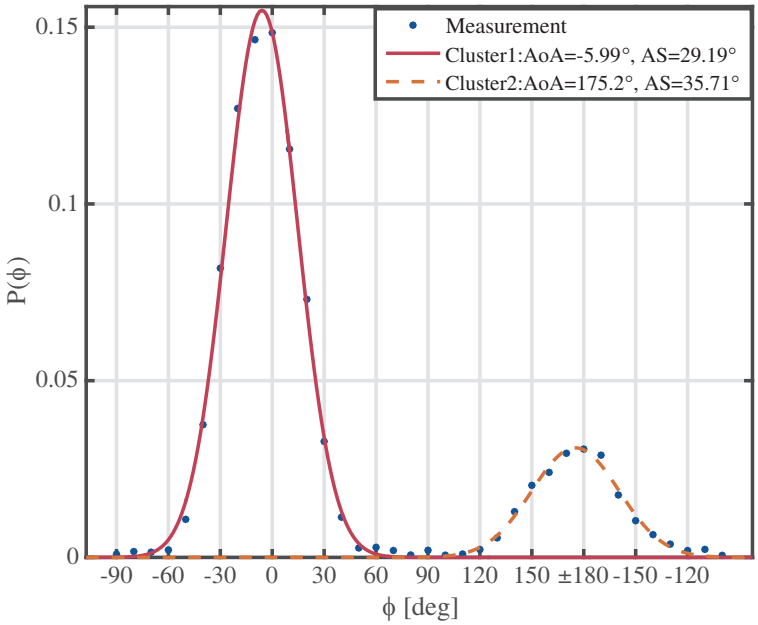

Figure 5. Co-polarized PAS for Tx-Rx distance of 75 m.

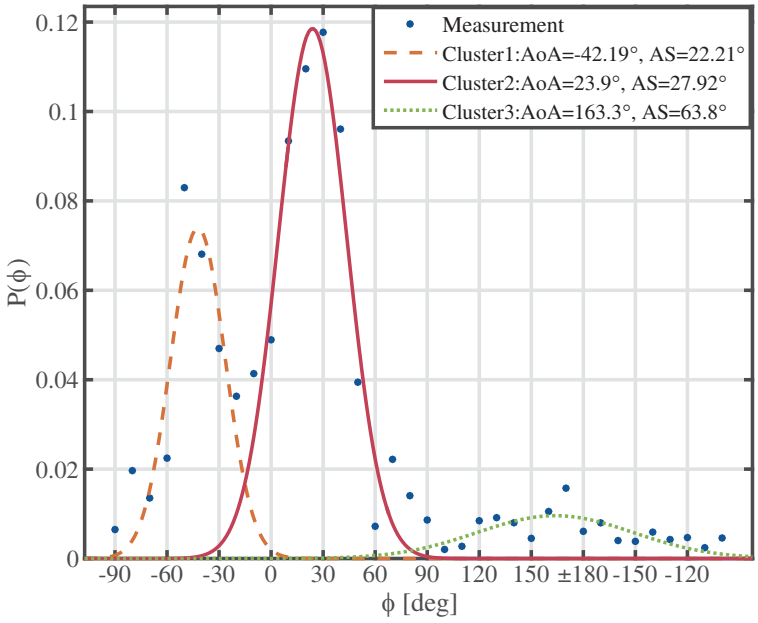

Figure 6. Cross-polarized PAS for Tx-Rx distance of 25 m.

propagation prediction commercially. The ray-tracing simulation parameters using WI was set according to Table 2. The tunnel walls are made of reinforced concrete material, and the specifications of the material are listed in Table 3. The material of the train was set to perfect conductor. The PAPs comparisons between simulation and measurements for any azimuth AoA and polarization for any Tx-Rx distance are normalized by the maximum MPC power, given in Fig. 8. Hence, 0 dB corresponds to the maximum MPC power of each plot. Many small objects are hanging on the sidewall, such as leaky cables and small metal boxes, which leads to the small differences between ray-tracing and measurement for cross-polarization in the tunnel. However, in most cases, the PAPs of simulation and measurement in the tunnel show good agreement.

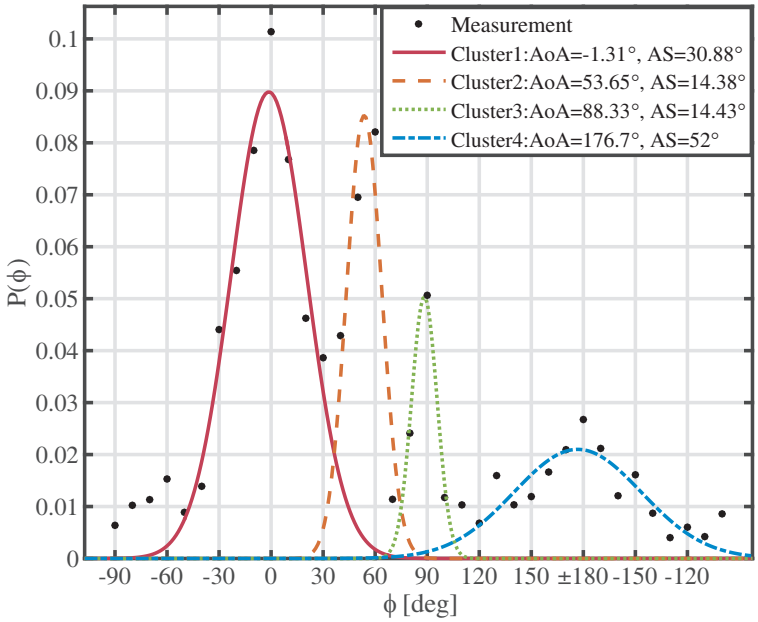

Figure 7. Cross-polarized PAS for Tx-Rx distance of 75 m.

Table 2. Ray-tracing simulation parameters.

Parameters	Value
Center frequency	1.8 GHz
Transmitting power	20 dBm
Number of reflection	30
Number of diffraction	0

Table 3. Material specifications of the tunnel in simulations.

Materials	Concrete
Conductivity (S/m)	0.04
Permittivity	5.31
Thickness (m)	0.5
Roughness (m)	0.001

For co-polarized configurations, MPCs are mainly around 0° (LOS direction) and 180° (RWET), which can be seen in Fig. 8(a) and Fig. 8(b). The waves propagations correspond to Fig. 9(a) and Fig. 9(b). Especially when the Rx antenna points to the tunnel sidewall and perpendicular to the tunnel axis, the co-polarized signals have lower received power. This is because the received signals experienced multi-reflection. As the Tx-Rx separation increases, the 180° MPCs become stronger, while the 0° component becomes weaker concurrently. The contribution of sidewall reflection signals becomes lower with the increase of the Tx-Rx distance for co-polarized signals. From Fig. 9(a) and Fig. 9(b), it can be seen that less RWS were received by the Rx at 75 m than the 25 m distance.

For cross-polarized configurations, the received power is lower than the co-polarizations. The main MPCs are the virtual LOS and RWET as shown in Fig. 8(c) and Fig. 8(d). The ray propagation in the tunnel is shown in Fig. 9(c) and Fig. 9(d). The 0° component is reflected from the ground and ceiling,

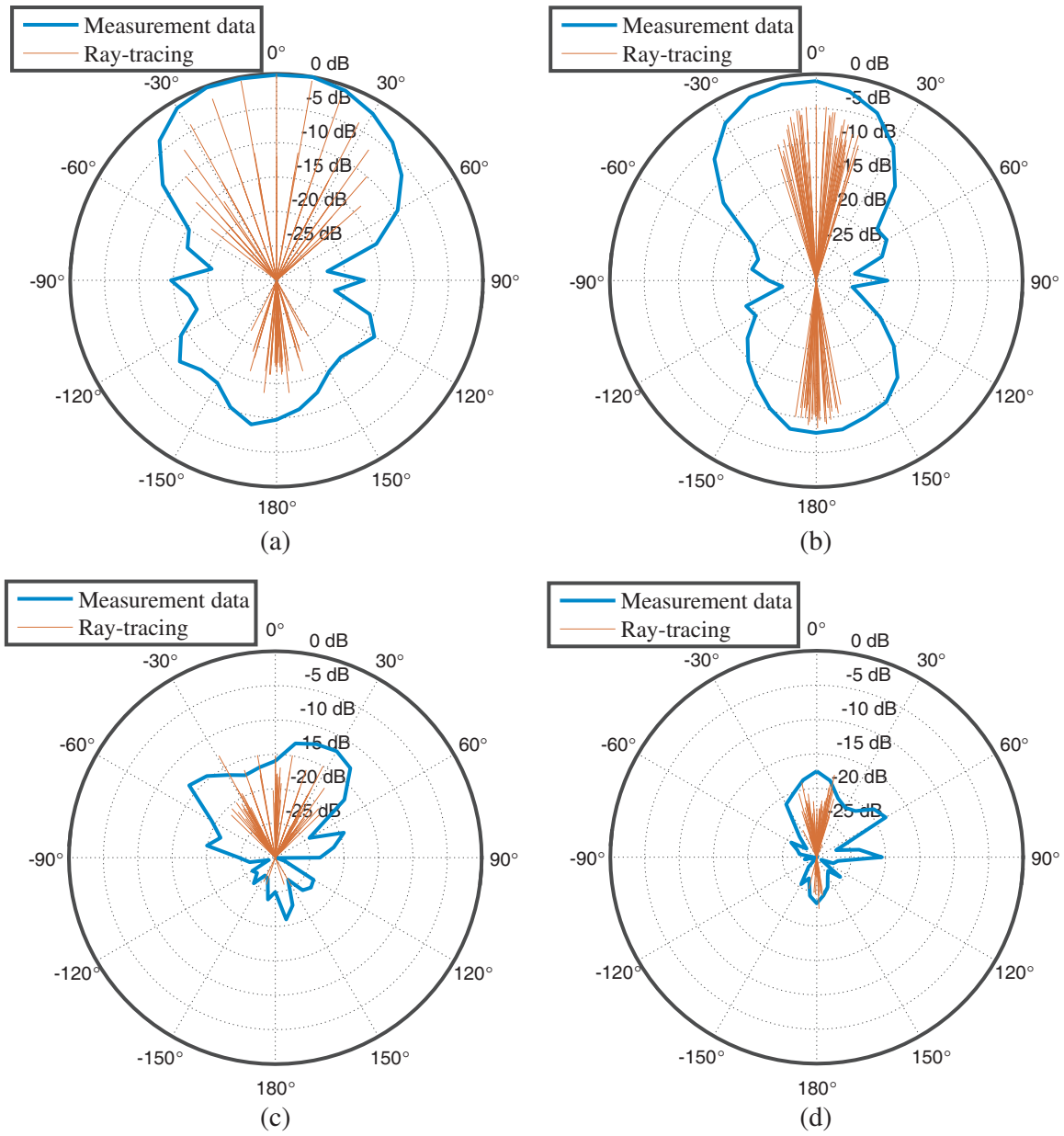

Figure 8. PAPs comparison between channel measurement and ray-tracing simulation in Nantong tunnel. (a) Co-polarized and Tx-Rx distance 25 m. (b) Co-polarized and Tx-Rx distance 75 m. (c) Cross-polarized and Tx-Rx distance 25 m. (d) Cross-polarized and Tx-Rx distance 75 m.

and the 180° component is the RWET. However at 25 m position of the Rx, the RWET is so weak that cannot be detected by the Rx. The 180° component is reflected from the tunnel junction.

An actual subway tunnel is usually longer than Nantong tunnel. The Hong Kong NS 173 subway tunnel in [16] was 3.43 m wide, 2.6 m high, and 258.7 m long. Nantong tunnel has a similar cross-section size as the Hong Kong NS 173 subway tunnel, but shorter in length. There is a metal door at the end of Nantong tunnel which is not present in regular subway tunnels, but could emulate the presence of a train. In order to verify the influence of the metal door at the end of the tunnel on the signal propagation, we created a 3D model whose first 100 m length has the same volume as Nantong tunnel, and then we placed a train with the size of 1.76 m (width) × 2.38 m (height) × 23 m (length) at 100 m away from the tunnel entrance, as can be seen in Fig. 10. The simulation results revealed that a good

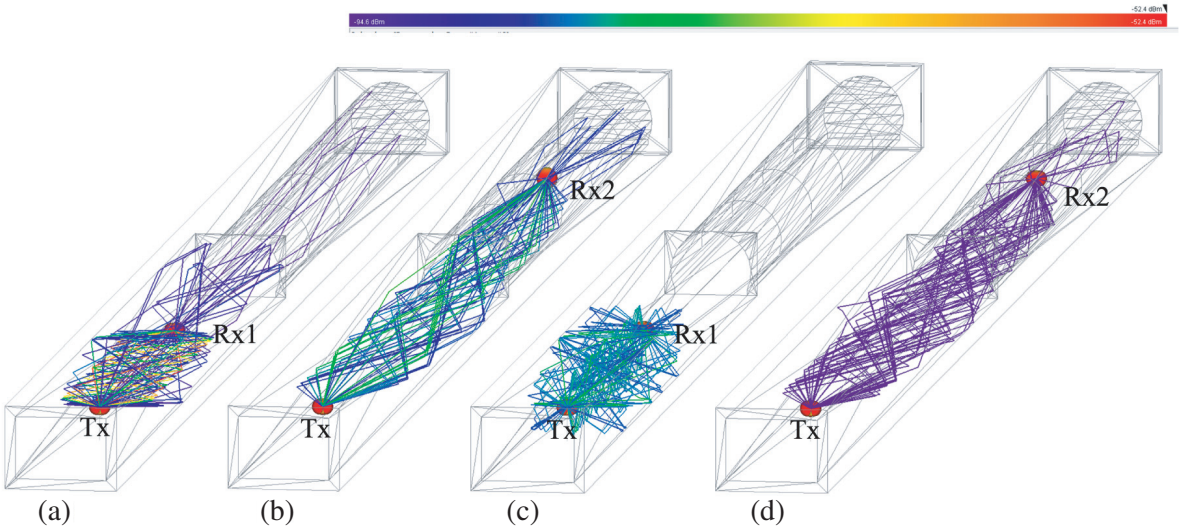

Figure 9. Rays propagation in Nantong tunnel with ray-tracing simulation. (a) Co-polarized and Tx-Rx distance 25 m. (b) Co-polarized and Tx-Rx distance 75 m. (c) Cross-polarized and Tx-Rx distance 25 m. (d) Cross-polarized and Tx-Rx distance 75 m.

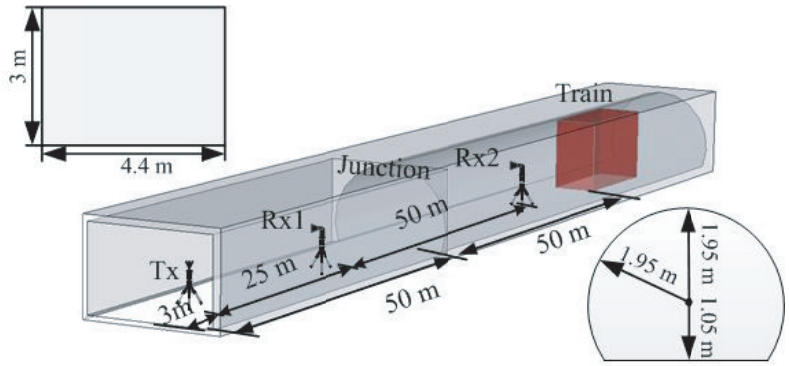

Figure 10. Ray-tracing simulation scenarios with a train in the tunnel.

agreement was achieved between Fig. 11 and Fig. 8. It can be seen that the door has nearly the same effect as the train on the signal propagation in the tunnel. Then we can conclude that the metal door at the end of the tunnel can be seen as a train, and the measurement results in the tunnel can be used to guide an actual tunnel with a train in it.

According to [17], spatial correlation coefficient can be calculated as

$$\rho(D) = R_{xx}(D) + jR_{xy}(D) \tag{3}$$

$$R_{xx}(D) = \frac{1}{M}\sum_{n=1}^{M}\left\{J_0(D) + Q_n\sum_{m=1}^{\infty}J_{2m}(D)e^{-2\sigma_n^2 m^2}\cos(2m\phi_n)\right.$$
$$\left.\cdot\mathbf{Re}\left[erf\left(\frac{\Delta\phi_n}{\sigma_n\sqrt{2}} - jm\sigma_n\sqrt{2}\right) - erf\left(\frac{-\Delta\phi_n}{\sigma_n\sqrt{2}} - jm\sigma_n\sqrt{2}\right)\right]\right\} \tag{4}$$

$$R_{yy}(D) = \frac{1}{M}\sum_{n=1}^{M}\left\{Q_n\sum_{m=1}^{\infty}J_{2m+1}(D)e^{-2\sigma_n^2(m+1/2)^2}\sin((2m+1)\phi_n)\right.$$
$$\left.\cdot\mathbf{Re}\left[erf\left(\frac{\Delta\phi_n}{\sigma_n\sqrt{2}}-j\sigma_n\sqrt{2}(m+1/2)\right)-erf\left(\frac{-\Delta\phi_n}{\sigma_n\sqrt{2}}-j\sigma_n\sqrt{2}(m+1/2)\right)\right]\right\} \quad (5)$$

where $D = 2\pi d/\lambda$, $J_m(\cdot)$ is the first-kind m-th order Bessel function, and $erf(\cdot)$ denotes an error function. The correlation coefficients of different antenna element spacings with co-polarization and cross-polarization at two Rx locations are illustrated in Fig. 12. As can be seen, for co-polarized configurations, the correlation coefficients follow an increasing function of the Tx-Rx distance, but for cross-polarized configurations, the correlation coefficients have an opposite trend. This is because the

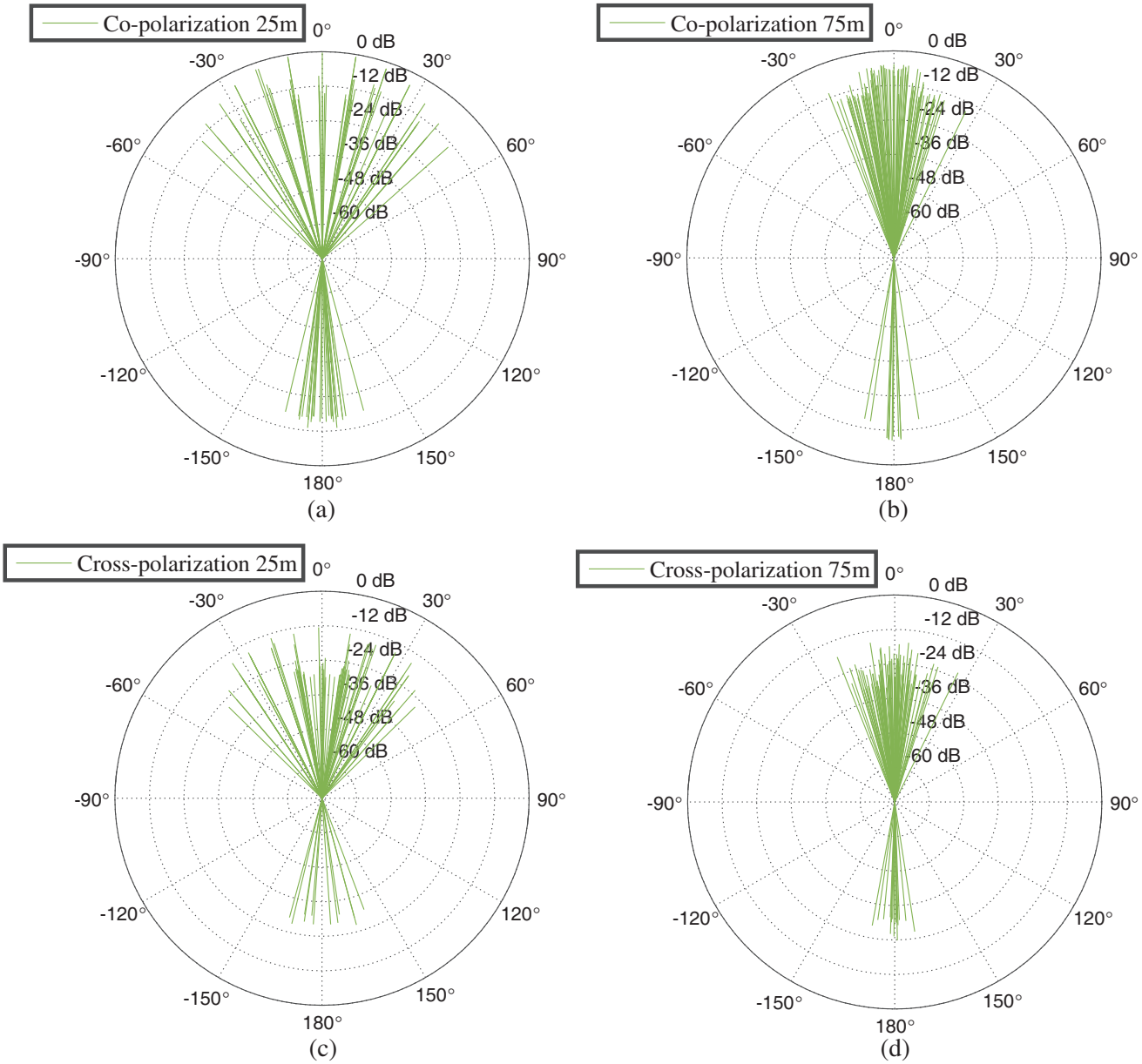

Figure 11. PAPs of ray-tracing simulation with a train in the tunnel. (a) Co-polarized and Tx-Rx distance 25 m. (b) Co-polarized and Tx-Rx distance 75 m. (c) Cross-polarized and Tx-Rx distance 25 m. (d) Cross-polarized and Tx-Rx distance 75 m.

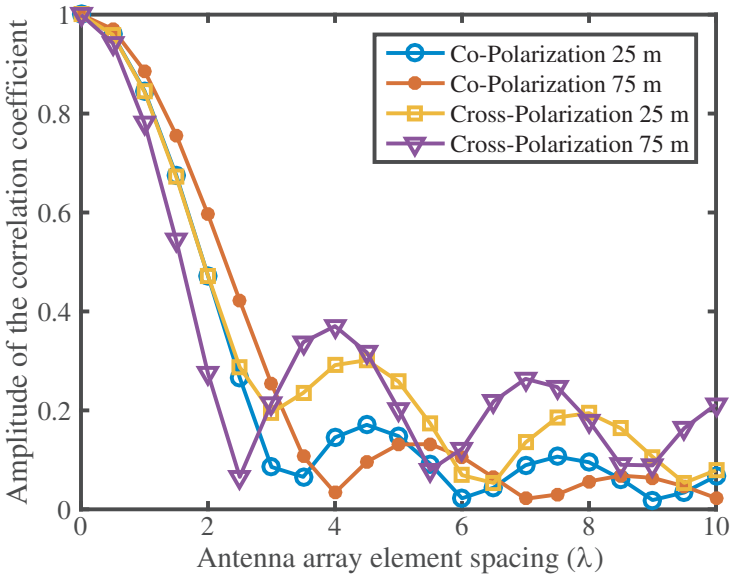

Figure 12. Correlation coefficient of different antenna elements spacing.

AS of maximum power cluster has a significant influence on the spatial correlation. We can see from Figs. 4–7 that the AS of the maximum power cluster with co-polarized configurations decreases with Tx-Rx distance, but increases with cross-polarized configurations.

4. CONCLUSION

In this paper, the channel measurements at 1.8 GHz are conducted in a subway-like tunnel in Nantong. The characterization of the angle and polarization of multipath channels have been investigated.

The RWET MPCs are partially depolarized. The cross-polarized MPCs decay faster than the co-polarized MPCs. The cross-polarized MPCs of RWET cannot be received by the Rx with shorter Tx-Rx distances. However, the power of the cross-polarized signals of RWS near the Rx is even higher than the co-polarized signals. Therefore, the maximum depolarized signals are the RWS, which explains why the scatters surrounding the Rx are the main source of the depolarization. The PAS for both polarization configurations has multi-cluster, and the PAS is accurately described by a Truncated Gaussian function. The number of clusters for co-polarization is less than the cross-polarization. The propagation rays in the tunnel were studied with a commercial ray-tracing software Wireless InSite. The results demonstrated that for all the measurement locations, the main MPCs are around LOS and RWET. RWS becomes insignificant with the increment of the Tx-Rx separation. From the ray-tracing simulation results we can see that the metal door at the other end of the tunnel has the same function as a train. The spatial correlation of the co-polarized configuration is an increasing function of Tx-Rx distance, but a decreasing function of the cross-polarized configuration.

ACKNOWLEDGMENT

We are grateful to the Zhongtian Technology Company (ZTT) for letting us use their model subway tunnel, located in Nantong, China [18]. This work was supported by the National Natural Science Foundation of China under Grant 61571282.

REFERENCES

1. Wang, H., F. R. Yu, and H. Jiang, "Modeling of radio channels with leaky coaxial cable for LTE-M based CBTC systems," *IEEE Communications Letters*, Vol. 20, No. 5, 1038–1041, 2016.

2. Hrovat, A., G. Kandus, and T. Javornik, "A survey of radio propagation modeling for tunnels," *IEEE Communications Surveys & Tutorials*, Vol. 16, No. 2, 658–669, 2014.
3. Forooshani, A. E., S. Bashir, D. G. Michelson, and S. Noghanian, "A survey of wireless communications and propagation modeling in underground mines," *IEEE Communications Surveys & Tutorials*, Vol. 15, No. 4, 1524–1545, 2013.
4. Lienard, M., P. Degauque, J. Baudet, and D. Degardin, "Investigation on MIMO channels in subway tunnels," *IEEE Journal on Selected Areas in Communications*, Vol. 21, No. 3, 332–339, 2003.
5. Forooshani, A. E., R. D. White, and D. G. Michelson, "Effect of antenna array properties on multiple-input-multiple-output system performance in an underground mine," *IET Microwaves, Antennas & Propagation*, Vol. 7, No. 13, 1035–1044, 2013.
6. Forooshani, A. E., C. Y. T. Lee, and D. G. Michelson, "Effect of antenna configuration on MIMO-based access points in a short tunnel with infrastructure," *IEEE Transactions on Communications*, Vol. 64, No. 5, 1942–1951, 2016.
7. Valdesueiro, J. A., B. Izquierdo, and J. Romeu, "On 2×2 MIMO observable capacity in subway tunnels at C-band an experimental approach," *IEEE Antennas and Wireless Propagation Letters*, Vol. 9, 1099–1102, 2010.
8. Molina-Garcia-Pardo, J. M., M. Lienard, P. Degauque, C. Garcia-Pardo, and L. Juan-Llacer, "MIMO channel capacity with polarization diversity in arched tunnels," *IEEE Antennas and Wireless Propagation Letters*, Vol. 8, 1186–1189, 2009.
9. Garcia-Pardo, C., J.-M. Molina-García-Pardo, M. Lienard, D. P. Gaillot, and P. Degauque, "Double directional channel measurements in an arched tunnel and interpretation using ray tracing in a rectangular tunnel," *Progress In Electromagnetics Research M*, Vol. 22, 91–107, 2012.
10. Forooshani, A. E., S. Noghanian, and D. G. Michelson, "Characterization of angular spread in underground tunnels based on the multimode waveguide model," *IEEE Transactions on Communications*, Vol. 62, No. 11, 4126–4133, 2014.
11. Sun, R., D. W. Matolak, C. Tao, L. Liu, Z. Tan, and T. Zhou, "Investigation of MIMO channel characteristics in a two-section tunnel at 1.4725 GHz," *International Journal of Antennas and Propagation*, Vol. 2017, 1–12, 2017.
12. L. Gurrieri, E., T. J. Willink, A. Petosa, and S. Noghanian, "Characterization of the angle, delay and polarization of multipath signals for indoor environments," *IEEE Transactions on Antennas and Propagation*, Vol. 56, No. 8, 2710–2719, 2008.
13. Truffer, P. and P. E. Leuthold, "Wide-band channel sounding at 24 GHz based on a novel fiber-optic synchronization concept," *IEEE Transactions on Microwave Theory and Techniques*, Vol. 49, No. 4, 692–700, 2001.
14. MacCartney, G., T. Rappaport, M. Samimi, and S. Sun, "Wideband millimeter-wave propagation measurements and channel models for future wireless communication system design," *IEEE Transactions on Communications*, Vol. 63, No. 9, 3029–3056, 2015.
15. Nie, X., J. Zhang, and P. Zhang, "Polarization and spatial statistics of wideband MIMO relay channels in urban environment at 2.35 GHz," *IEICE Transactions on Communications*, Vol. 94-B, No. 1, 139–149, 2011.
16. Zhang, Y. P., Y. Hwang, and R. G. Kouyoumjian, "Ray-optical prediction of radio-wave propagation characteristics in tunnel environments. 2. Analysis and measurements," *IEEE Transactions on Antennas and Propagation*, Vol. 46, No. 9, 1337–1345, 1998.
17. Schumacher, L., K. I. Pedersen, and P. E. Mogensen, "From antenna spacings to theoretical capacities — guidelines for simulating MIMO systems," *The 13th IEEE International Symposium on Personal, Indoor and Mobile Radio Communications*, Vol. 2, No. 2, 587–592, 2002.
18. http://www.zttcable.com.